Electronic Supplementary Material (ESI) for Journal of Materials Chemistry A.


*Electronic Supporting Information*

# Neutral $d^8$ Metal Complexes with Intervalence Charge-Transfer Transition Triggers Effective NIR-II Photothermal Conversion for Solar-Driven Desalination

Yung-Cong Yang,[†,#] Joanna S. Lin,[†,#] and Jen-Shyang Ni[†]*

[†] *Department of Chemical and Materials Engineering, Photo-sensitive Material Advanced Research and Technology Center (Photo-SMART), National Kaohsiung University of Science and Technology, Kaohsiung 80778, Taiwan*

[#] *These authors contributed equally to this work*

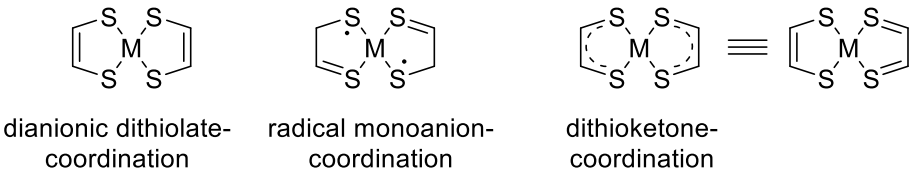


**Scheme S1.** The three coordination forms of neutral $d^8$ metal bis-dithiolene complexes. (M = Ni, Pd, Pt)

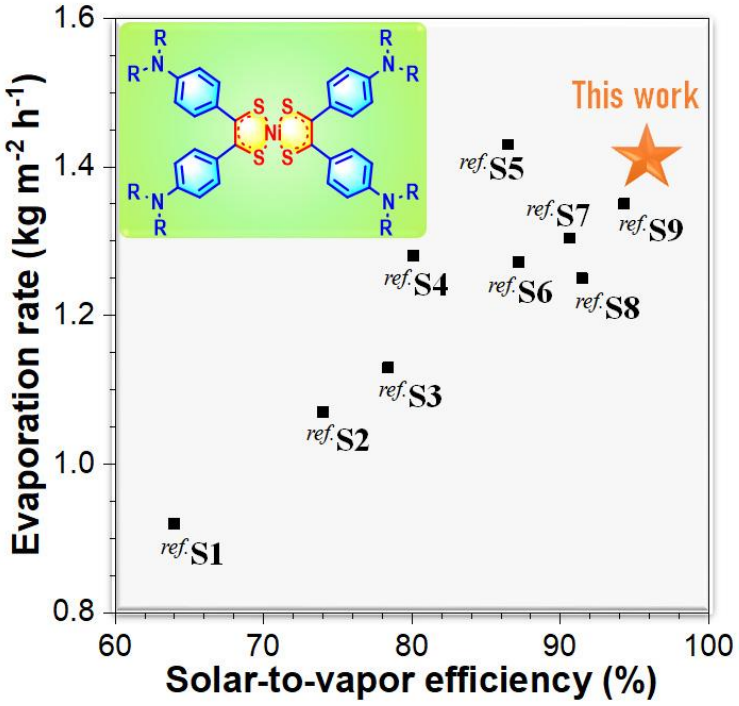


**Scheme S2.** The solar energy-to-vapor efficiency and water-mass evaporation rate of solar-thermal conversion materials based on small molecules.[S1-S9]

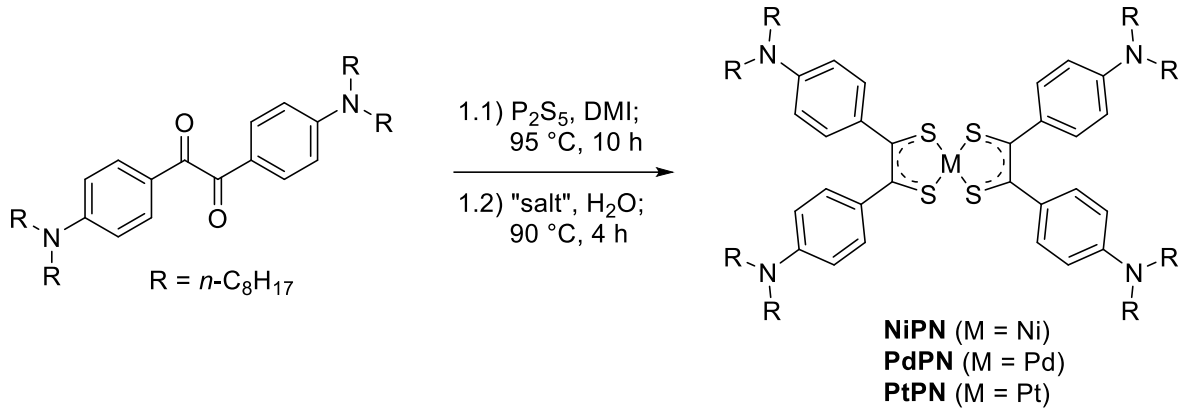


**Scheme S3.** Synthetic routes of neutral $d^8$ transition-metal bis-dithiolene complexes. The "salt" is $NiCl_2 \cdot 6H_2O$ for NiPN, $Na_2PdCl_4$ for PdPN, and $K_2PtCl_4$ for PtPN, respectively.

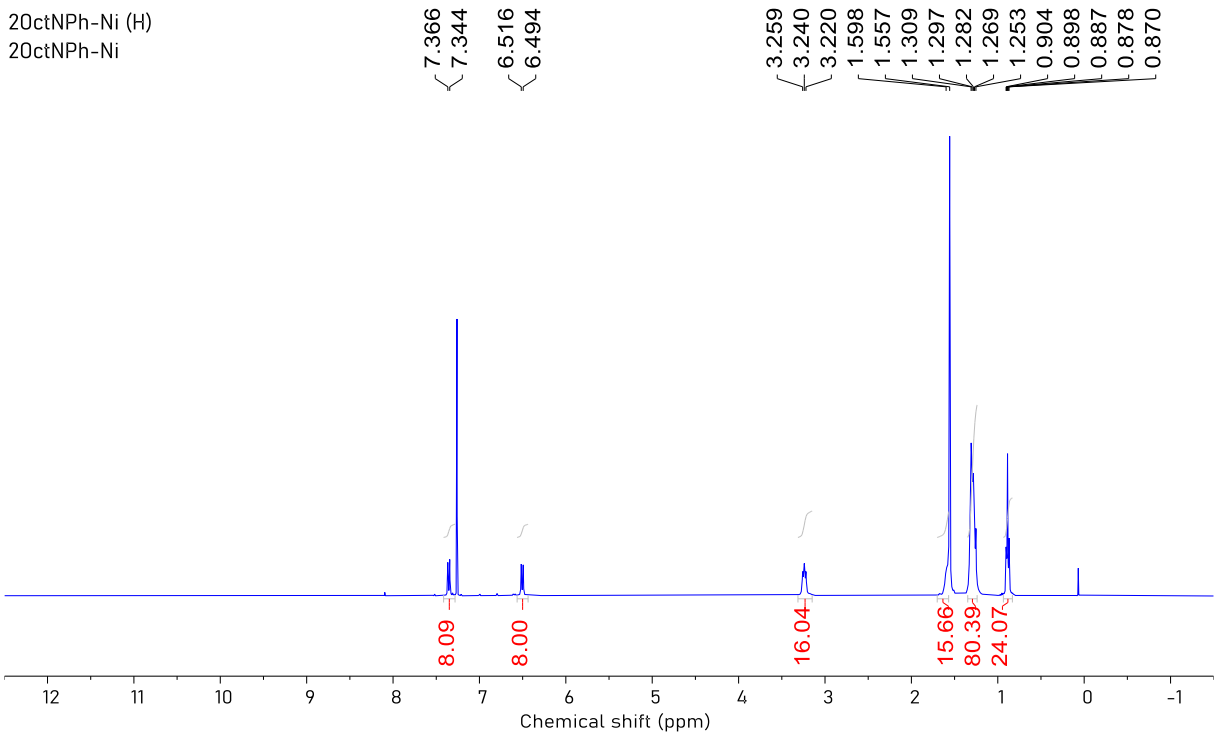


**Figure S1.** The $^{1}$H-NMR spectrum of NiPN in $CDCl_3$.

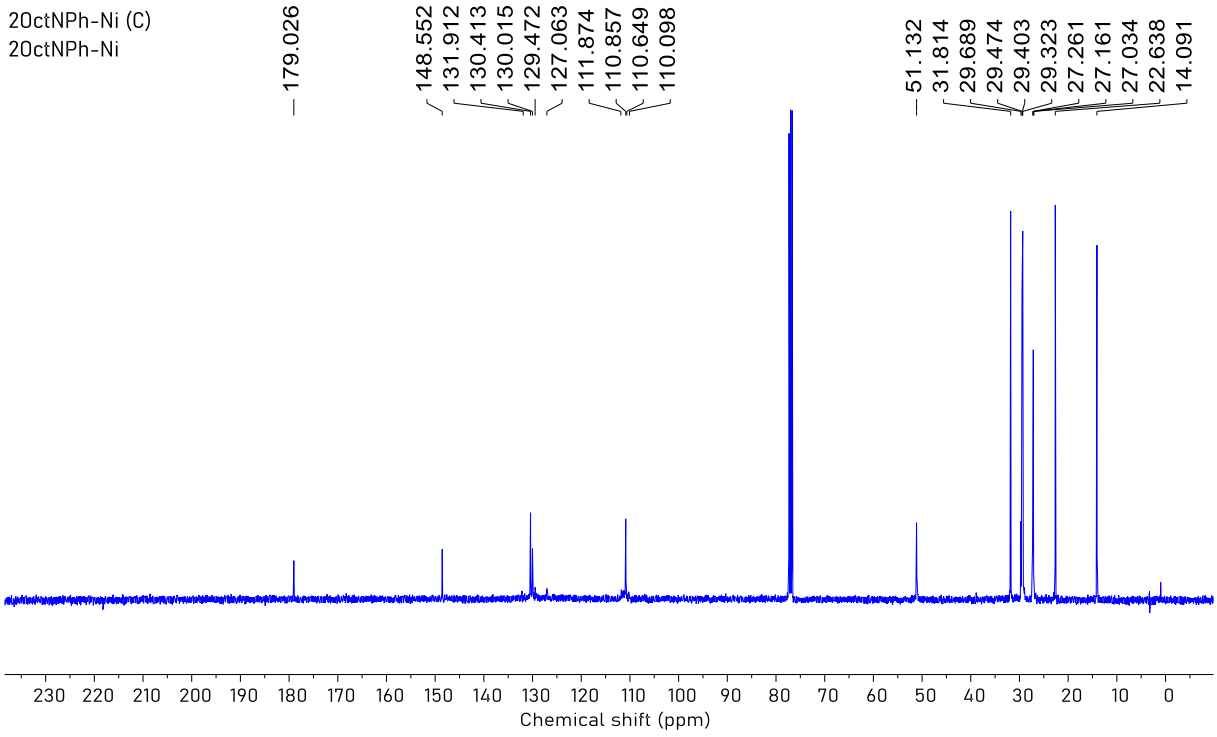


**Figure S2.** The $^{13}$C-NMR spectrum of NiPN in $CDCl_3$.

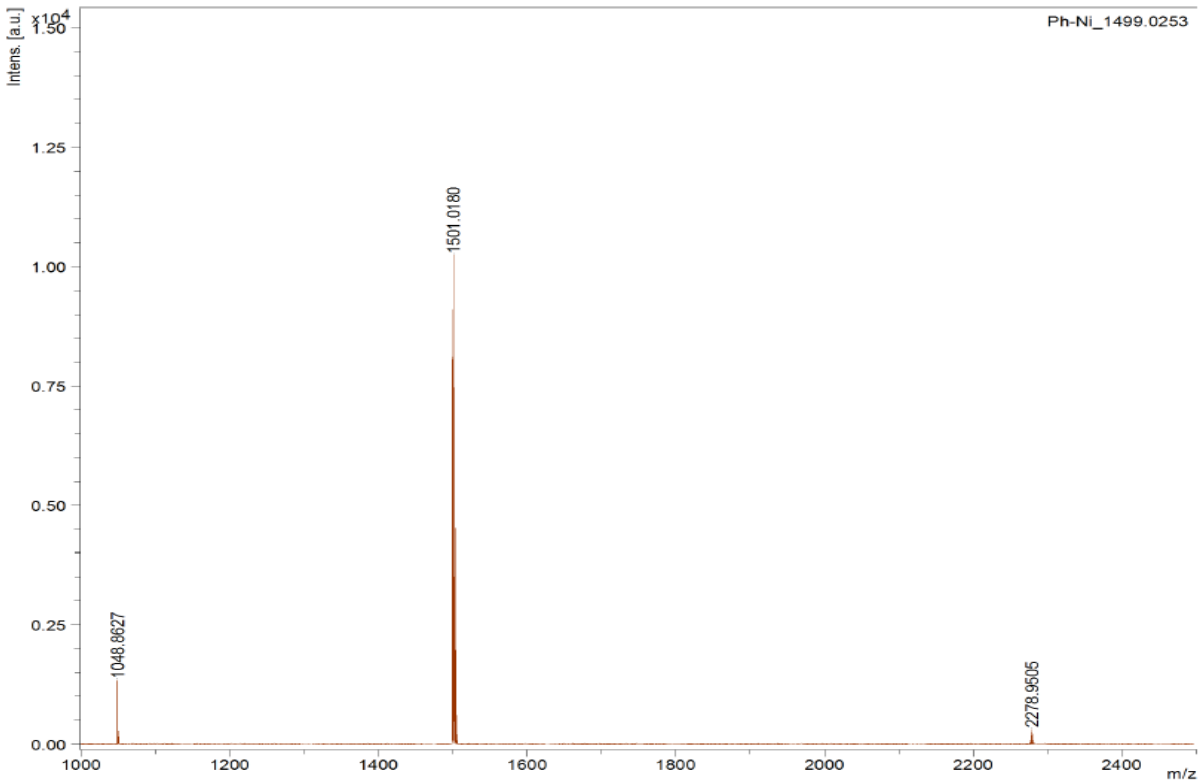


**Figure S3.** High-resolution mass spectrum of NiPN.

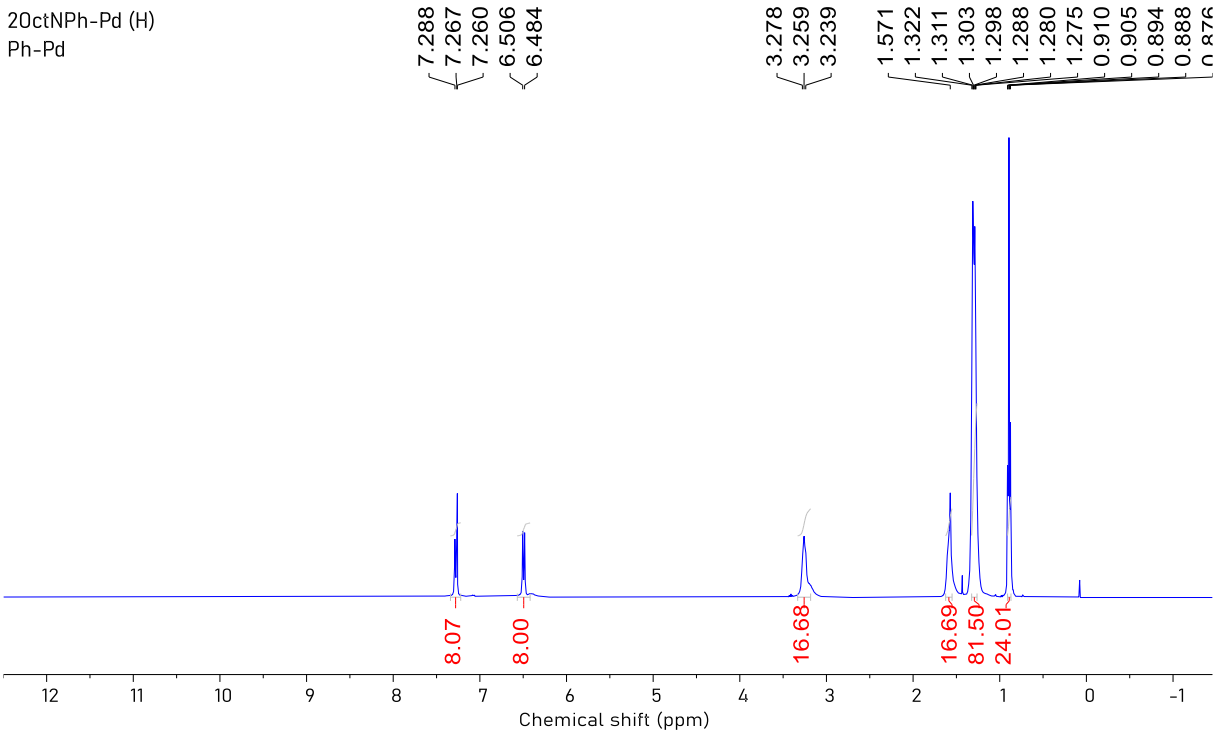


**Figure S4.** The $^{1}$H-NMR spectrum of PdPN in $CDCl_3$.

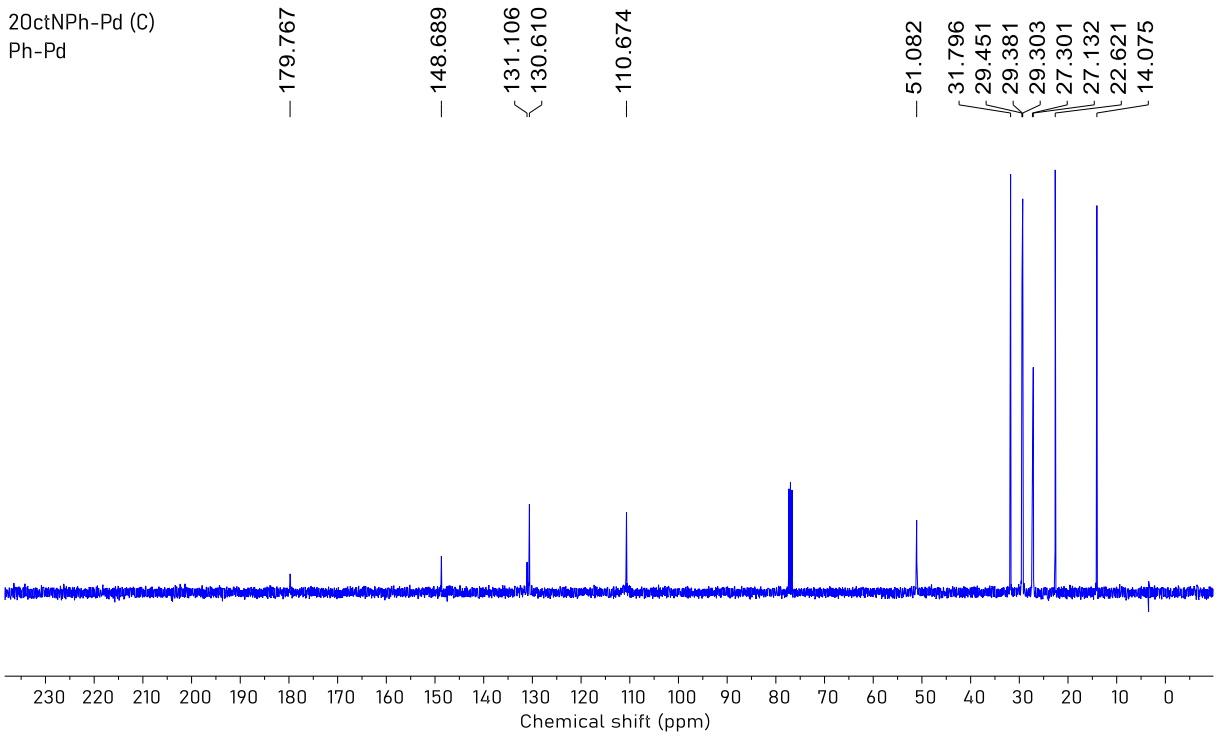


**Figure S5.** The $^{13}$C-NMR spectrum of PdPN in $CDCl_3$.

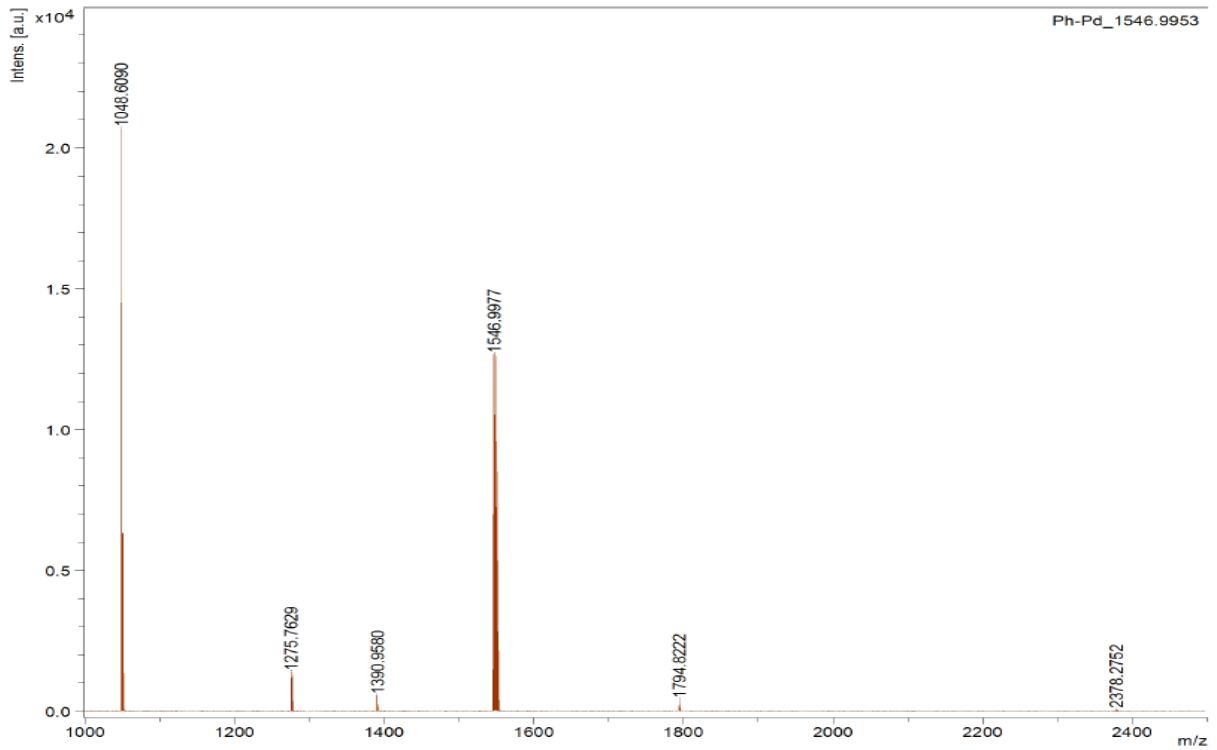


**Figure S6.** High-resolution mass spectrum of PdPN.

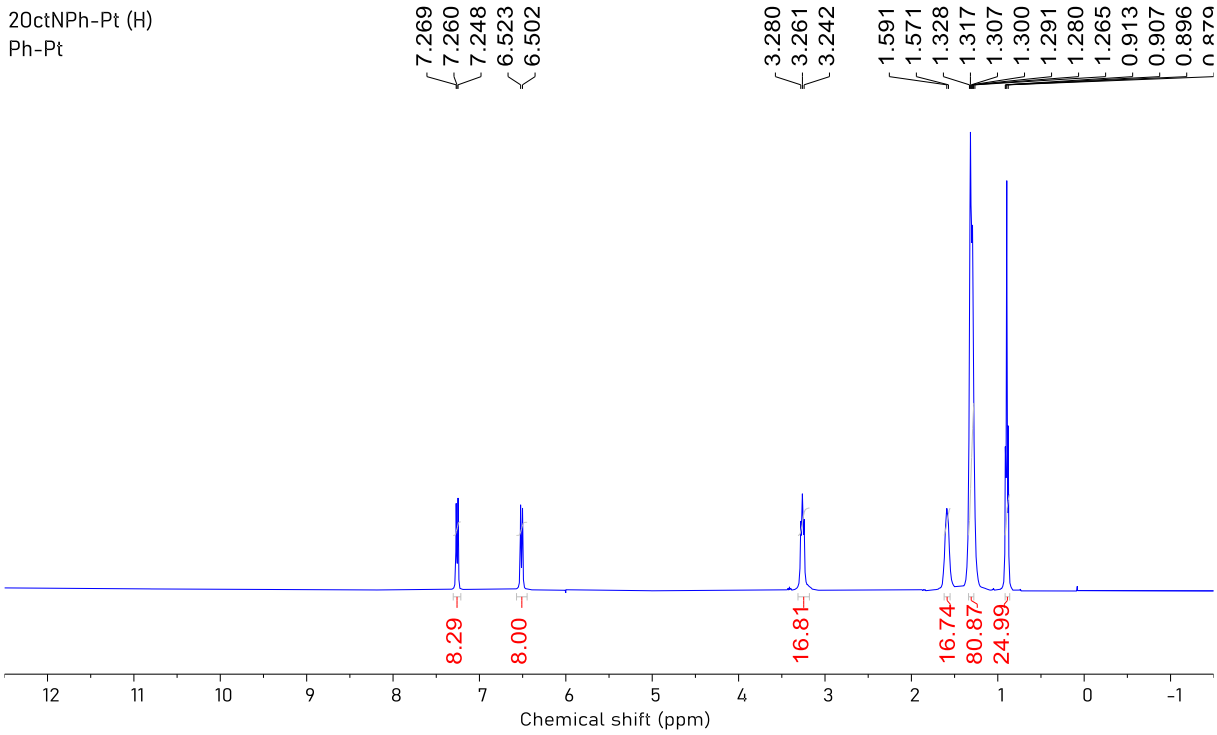


**Figure S7.** The $^{1}$H-NMR spectrum of PtPN in $CDCl_3$.

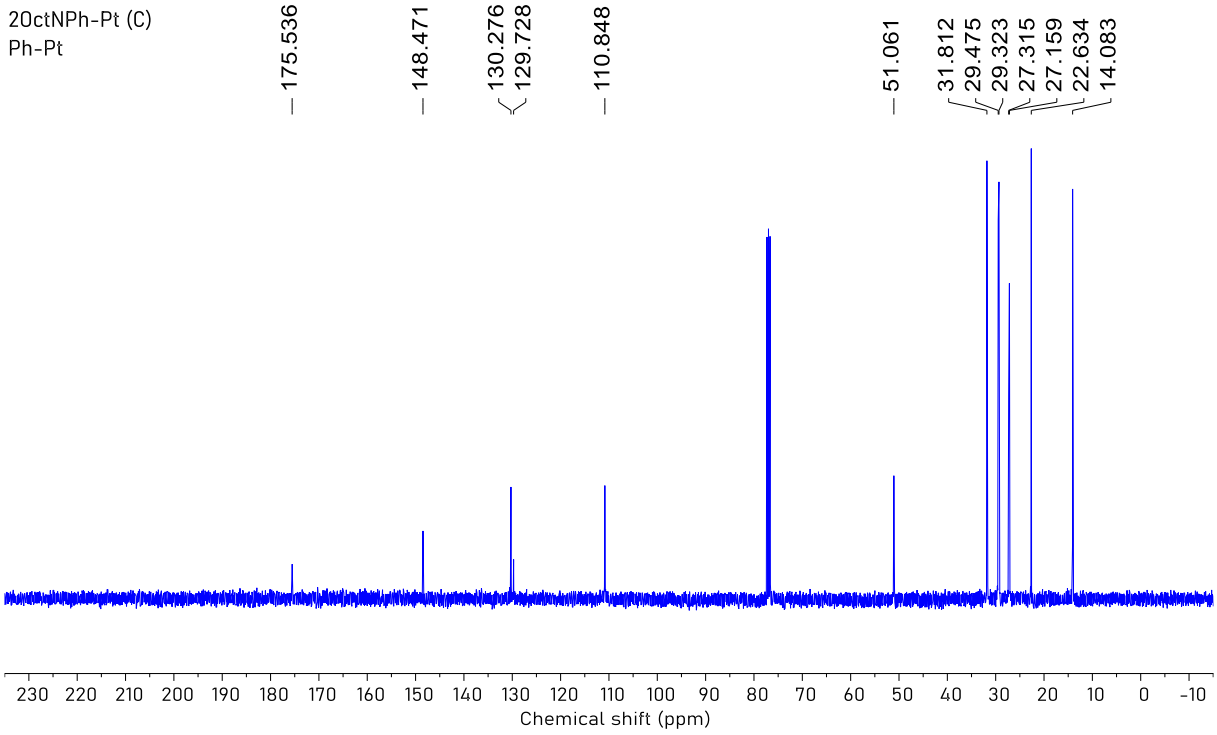


**Figure S8.** The $^{13}$C-NMR spectrum of PtPN in $CDCl_3$.

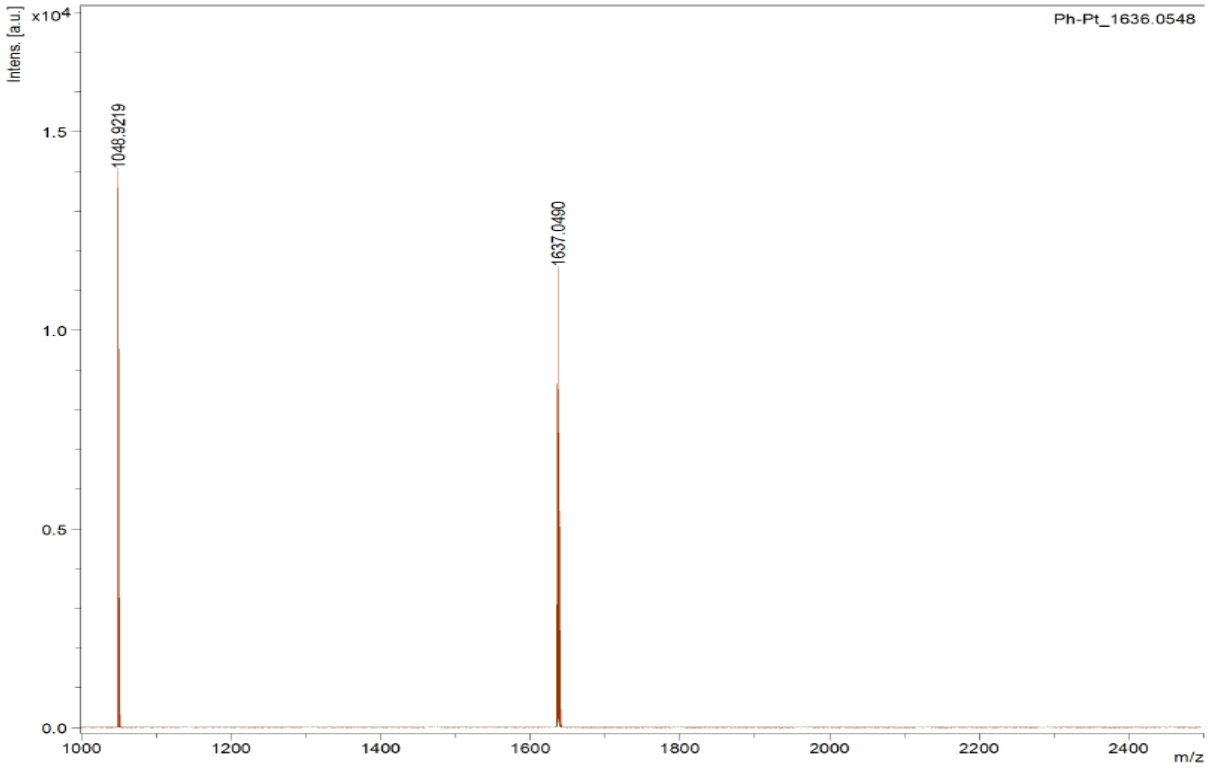


**Figure S9.** High-resolution mass spectrum of PtPN.

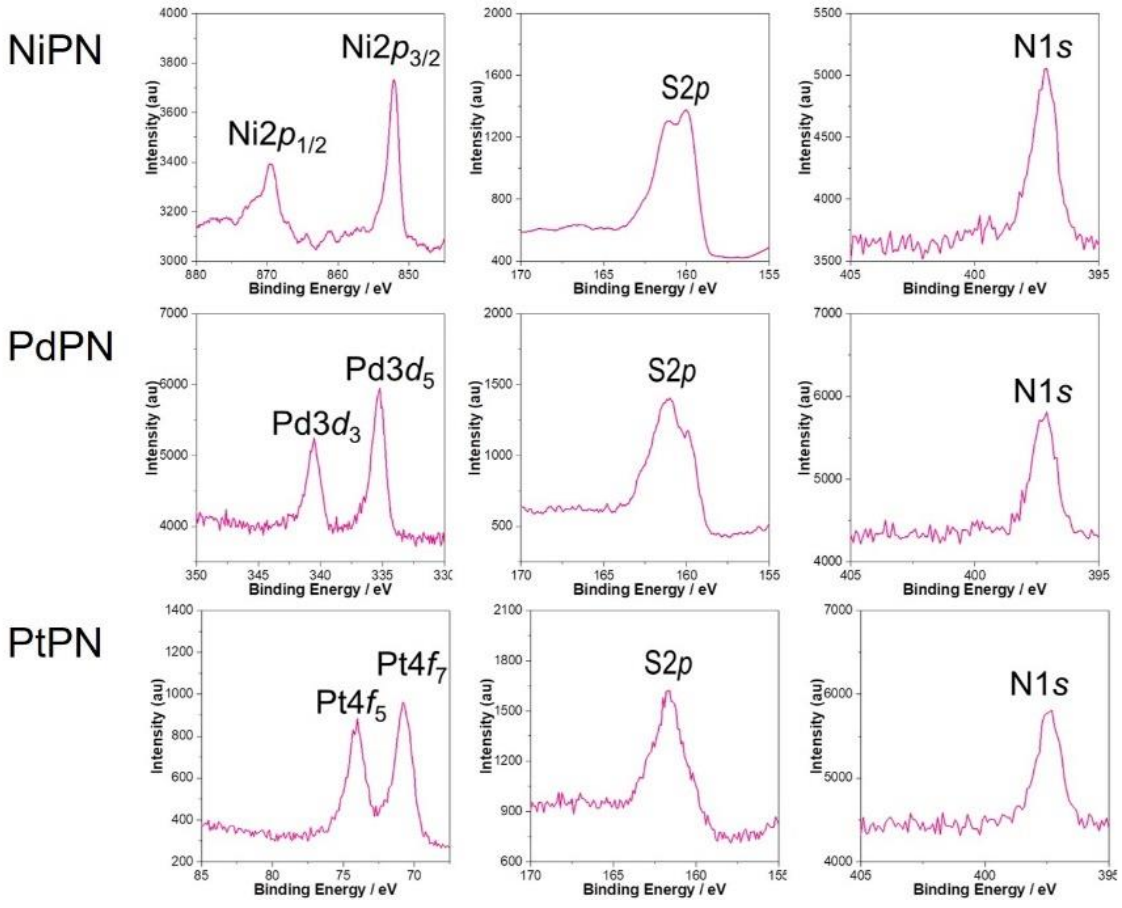


**Figure S10**. X-ray photoelectron spectroscopy (XPS) spectra of NiPN, PdPN, and PtPN powders.

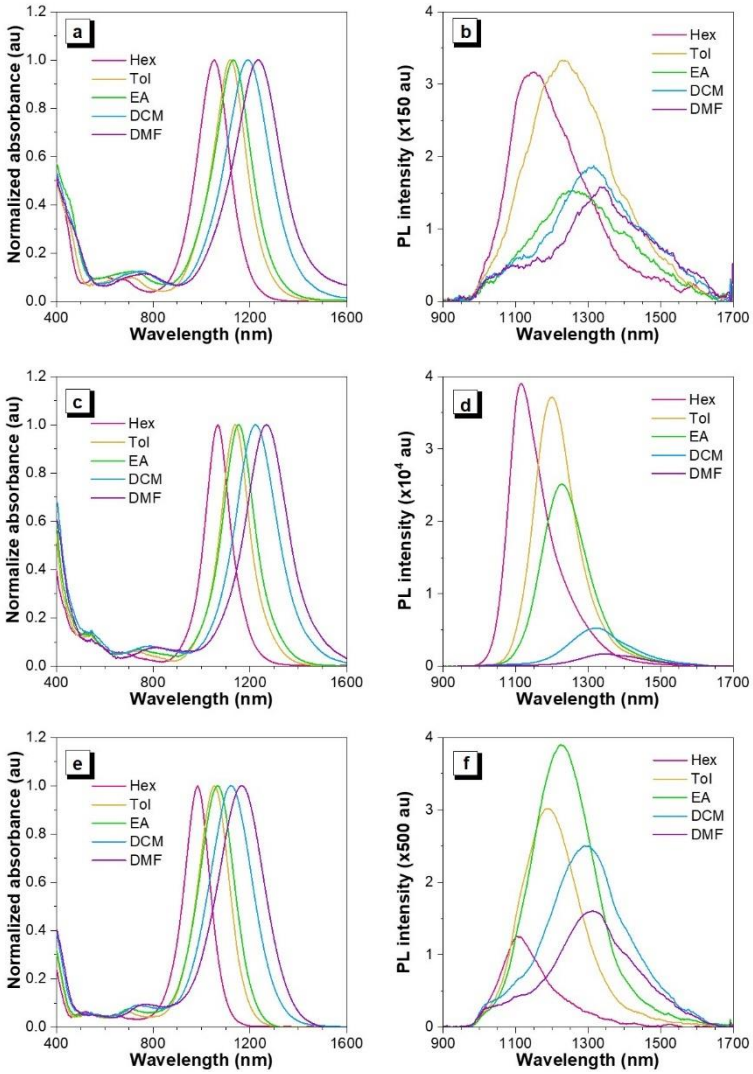


**Figure S11.** (a, c, and e) Normalized UV-vis-NIR absorption and (b, d, and f) PL spectra of NiPN (a, b), PdPN (c, d), and PtPN (e, f), respectively, in the different solvents (10 μM). The excitation wavelength is 808 nm. (Hex: hexane; Tol: toluene; EA: ethyl acetate; DCM: dichloromethane; DMF: dimethylformamide)

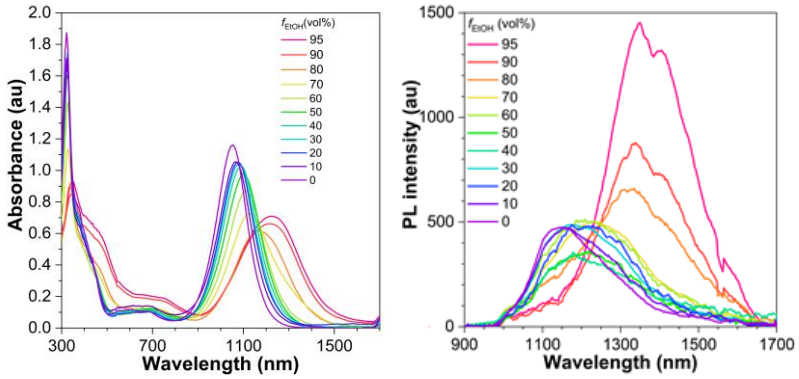


**Figure S12.** UV-vis-NIR absorption and PL spectra of NiPN with the different fractions of EtOH and hexane ($f_{EtOH}$, vol%) at a concentration of 10 μM. The excitation wavelength is 808 nm.

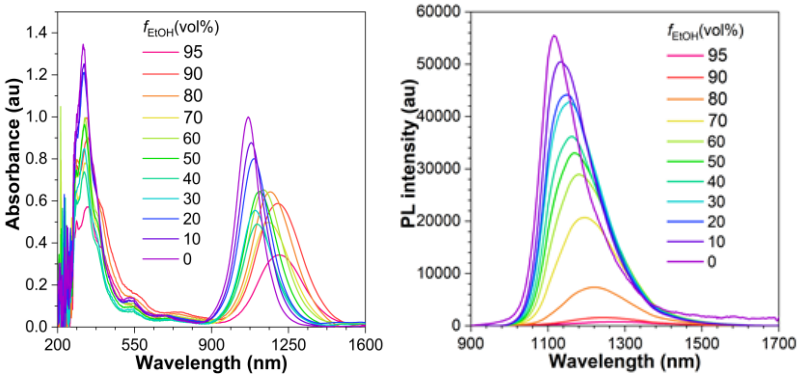


**Figure S13.** UV-vis-NIR absorption and PL spectra of PdPN with the different fractions of EtOH and hexane ($f_{EtOH}$, vol%) at a concentration of 10 μM. The excitation wavelength is 808 nm.

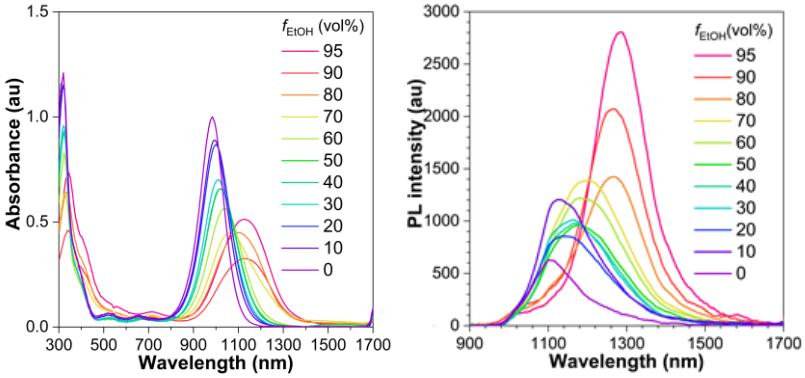


**Figure S14.** UV-vis-NIR absorption and PL spectra of PtPN with the different fractions of EtOH and hexane ($f_{EtOH}$, vol%) at a concentration of 10 μM. The excitation wavelength is 808 nm.

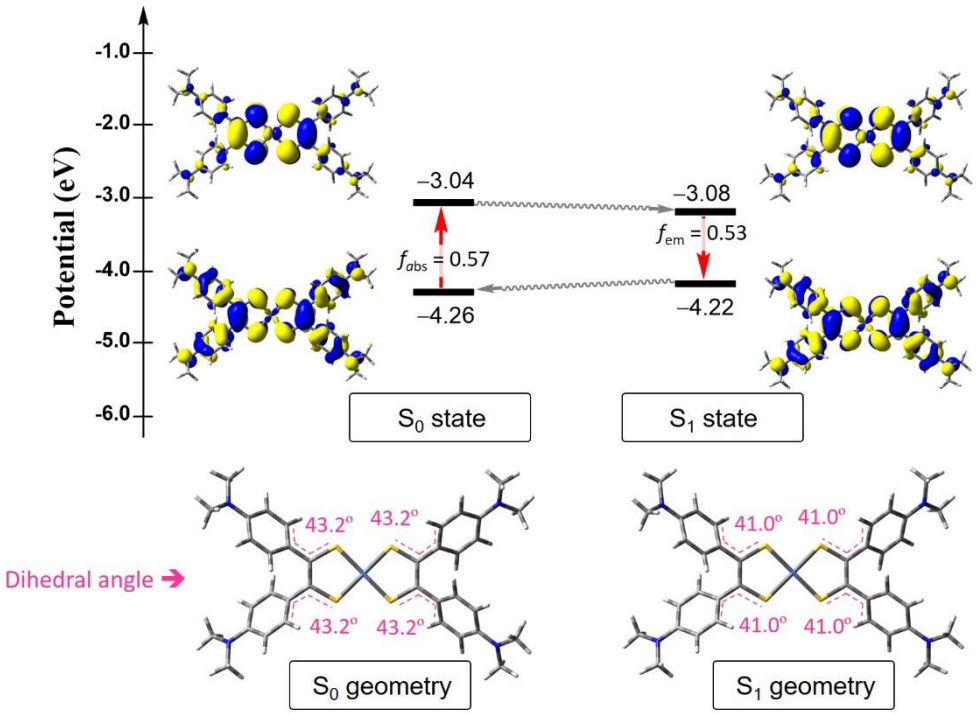


**Figure S15**. Molecular geometries, orbitals with isovalue of 0.02 a.u., energy levels, and dihedral angles of NiPN in the ground ($S_0$) and excited ($S_1$) states, calculated with TD-DFT at the level of B3LYP/6-31G(d)/LANL2DZ.

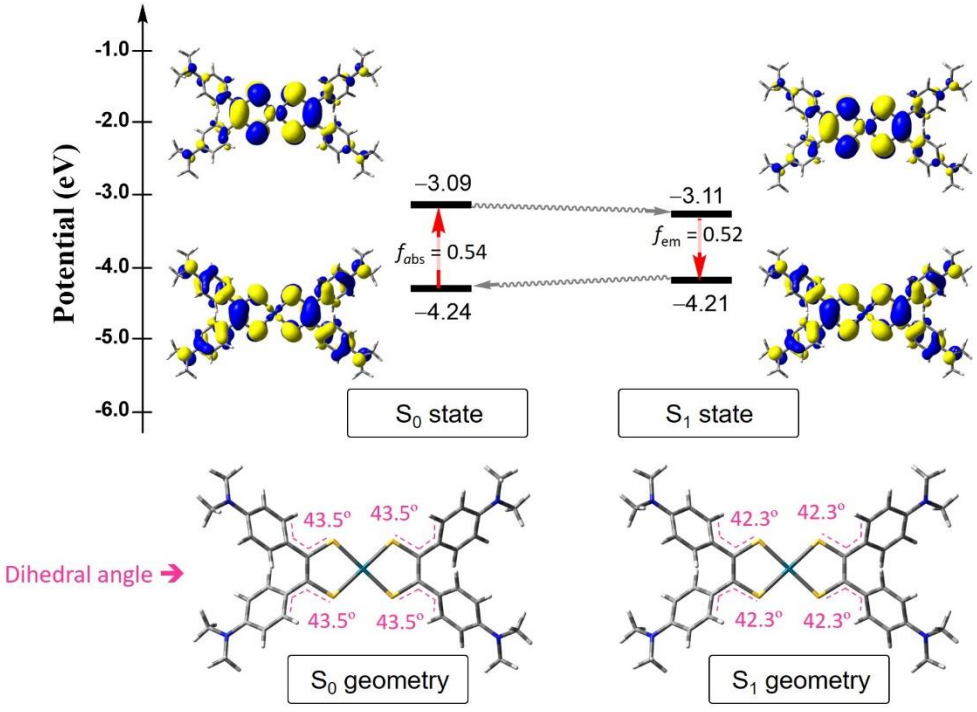


**Figure S16**. Molecular geometries, orbitals with isovalue of 0.02 a.u., energy levels, and dihedral angles of PdPN in the ground ($S_0$) and excited ($S_1$) states, calculated with TD-DFT at the level of B3LYP/6-31G(d)/LANL2DZ.

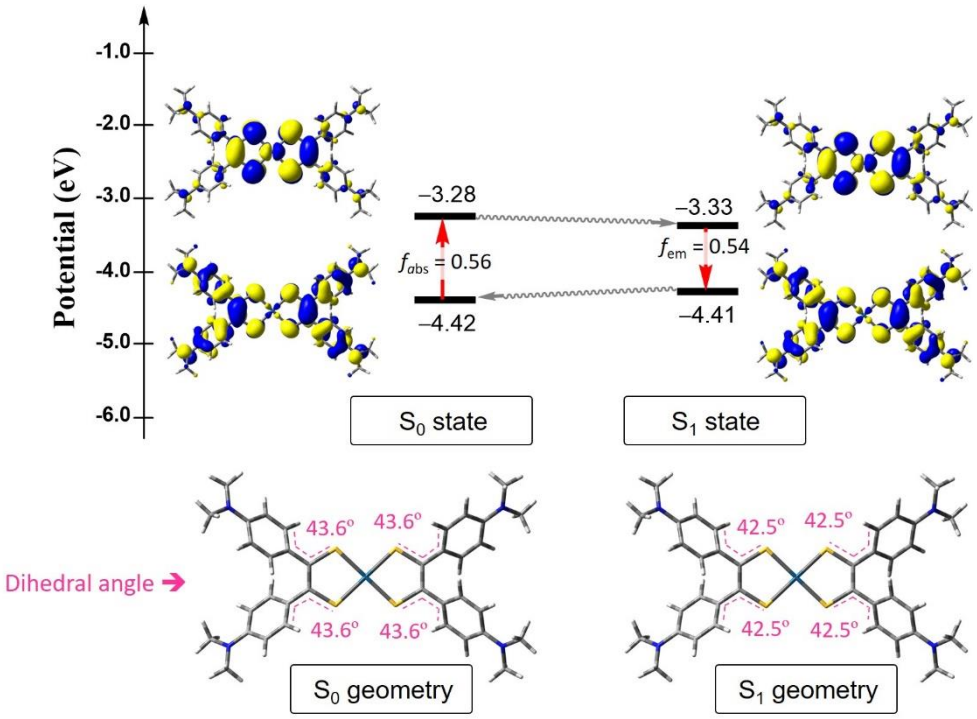


**Figure S17**. Molecular geometries, orbitals with isovalue of 0.02 a.u., energy levels, and dihedral angles of PtPN in the ground ($S_0$) and excited ($S_1$) states, calculated with TD-DFT at the level of B3LYP/6-31G(d)/LANL2DZ.

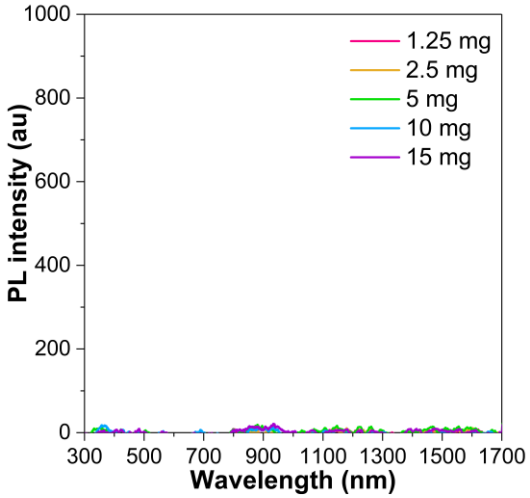


**Figure S18**. PL spectra of NiPN-adsorbed filter papers under the excitation wavelength of 808 nm.

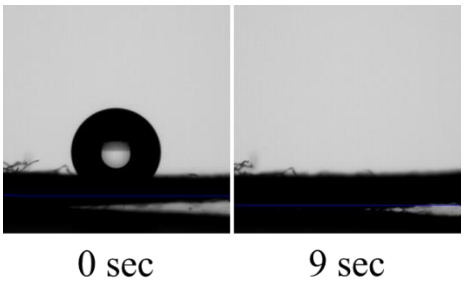


**Figure S19.** The time-dependent water contact angle (WCA) images of 1.25 mg of NiPN-loading filter papers.

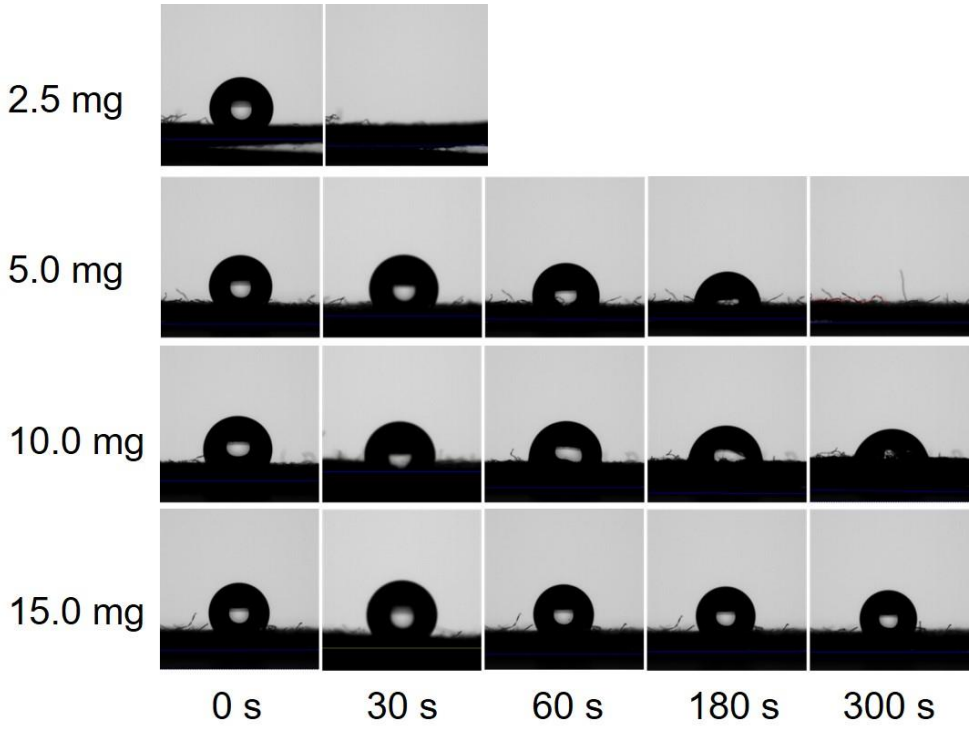


**Figure S20.** The time-dependent WCA images of NiPN-loading filter papers with different amounts, 2.5, 5.0, 10.0, and 15.0 mg, respectively.

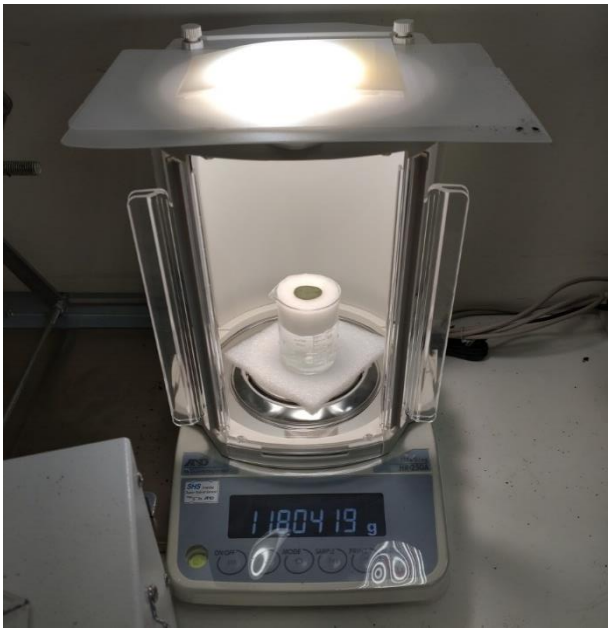

**Figure S21.** Camera photos of solar-driven evaporation device.

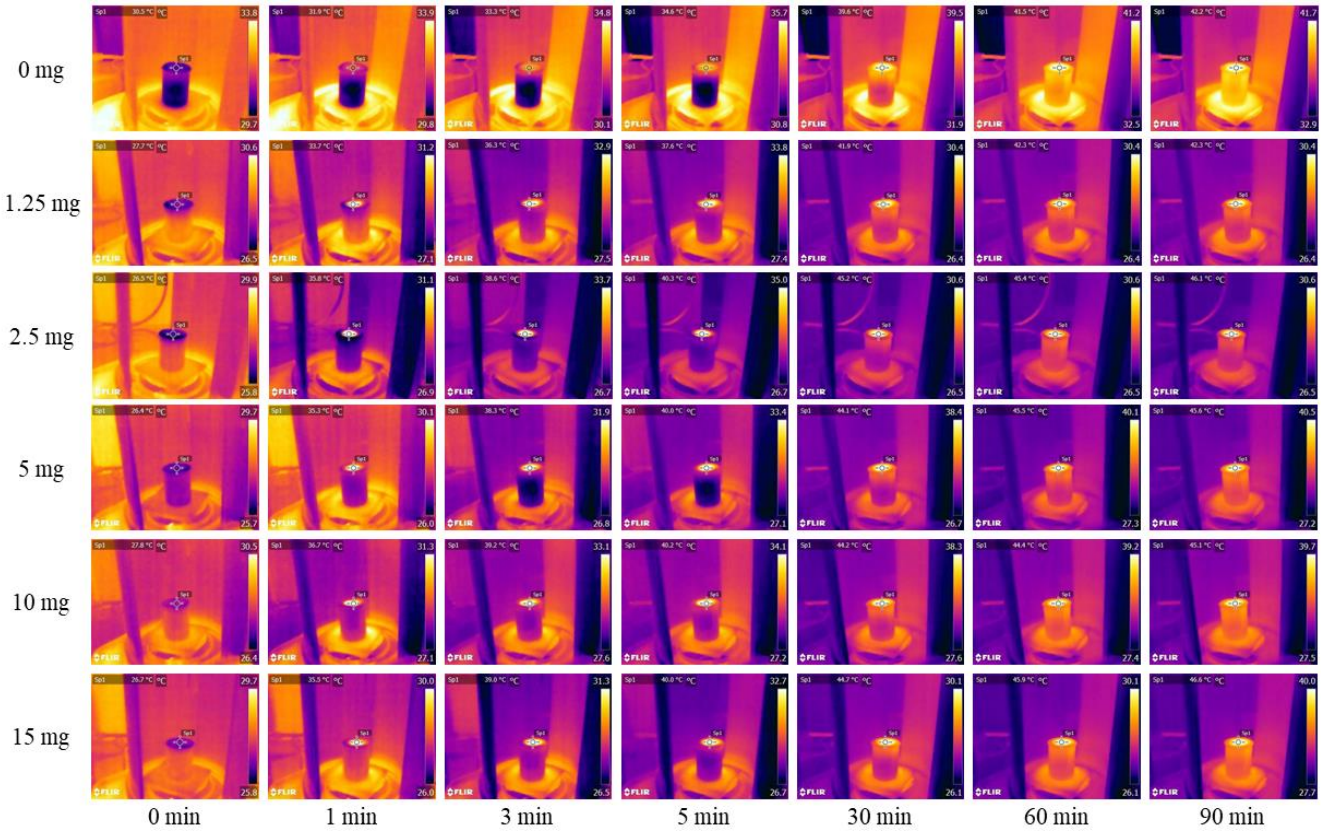


**Figure S22.** Infrared images of the solar-thermal interfacial-heating evaporation layers adsorbed with the different amounts of NiPN under 1 sun irradiation during time.

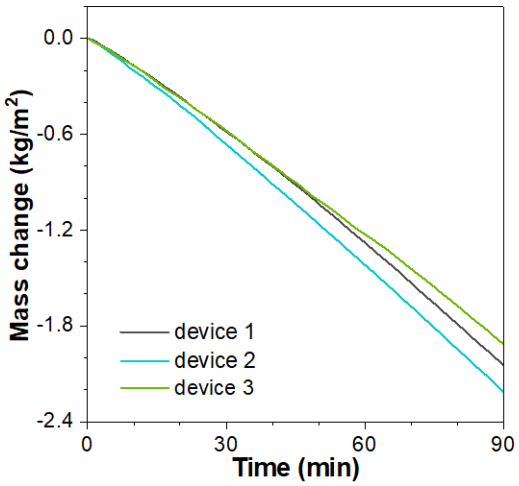


**Figure S23.** Time-dependent water-mass change curves using 2.5 mg of activated carbon-loading device under 1 sun irradiation.

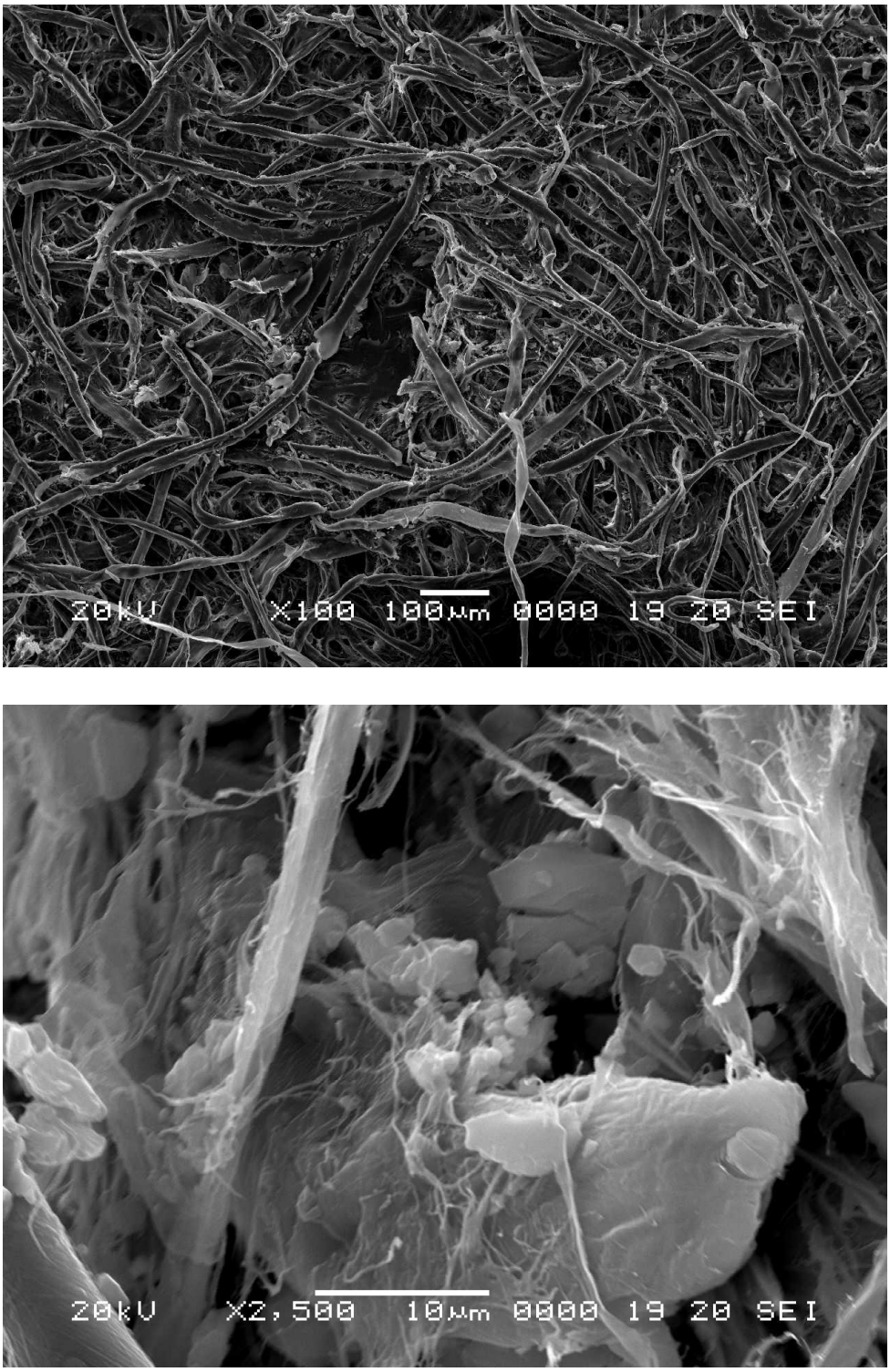


**Figure S24.** Scanning electron microscope images of NiPN loading filter paper, i.e., NiNP-adsorbed evaporators.

**Table S1**. Calculation data of organometallic complexes in $S_0$ state.

| Molecules | States | Configurations | $E$ (eV) | $\lambda$ (nm) | $f_{os}$ |
|---|---|---|---|---|---|
| NiNP | $S_{01}$ | H → L (96%) | 1.18 | 1050.05 | 0.565 |
| | $S_{02}$ | H–7 → L+1 (3%), H–5 → L (12%), H–2 → L (83%) | 1.52 | 818.26 | 0.002 |
| | $S_{03}$ | H–6 → L (3%), H–1 → L (91%), H → L+1 (6%) | 1.56 | 796.62 | 0.000 |
| PdNP | $S_{01}$ | H → L (96%) | 1.13 | 1093.18 | 0.536 |
| | $S_{02}$ | H–6 → L (4%), H–1 → L (92%), H → L+1 (4%) | 1.52 | 818.24 | 0.000 |
| | $S_{03}$ | H–5 → L (2%), H–2 → L (97%) | 1.55 | 798.16 | 0.004 |
| PtNP | $S_{01}$ | H → L (97%) | 1.09 | 1136.01 | 0.563 |
| | $S_{02}$ | H–5 → L (6%), H–2 → L (93%) | 1.33 | 931.58 | 0.002 |
| | $S_{03}$ | H–1 → L (98%) | 1.42 | 875.25 | 0.000 |

* Calculated with TD-DFT at the level of B3LYP/6-31G(d)/LANL2DZ. $S_{01}$, $S_{02}$, and $S_{03}$ denoted the first, second, and third vertical transition from the $S_0$ state to the $S_1$, $S_2$, and $S_3$, respectively, and $f_{os}$ denoted oscillator strength between the ground and excited states.

**Table S2**. Calculation data of organometallic complexes in $S_0$ state.

| Molecules | States | Configurations | $E$ (eV) | $\lambda$ (nm) | $f_{os}$ |
|---|---|---|---|---|---|
| NiNP | $S_{10}$ | H → L (96%) | 1.12 | 1111.46 | 0.534 |
| PdNP | $S_{10}$ | H → L (96%), H–6 → L+1 (2%) | 1.09 | 1140.88 | 0.520 |
| PtNP | $S_{10}$ | H → L (98%) | 1.04 | 1187.31 | 0.536 |

Calculated with TD-DFT at the level of B3LYP/6-31G(d)/LANL2DZ. $S_{10}$ denoted the first vertical transition from the $S_1$ to $S_0$ states, and $f_{os}$ denoted oscillator strength between the ground and excited states.

**Supporting References**


S1 Wang, D.; Qi, S.; Dong, J.; Wang, X.; Zhang, Y.; Zhou, S.; Gu, P.; Jia, T.; Zhang, Q., *Org. Lett.* **2023,** *25*, 5730-5734.

S2 Cui, Y.; Liu, J.; Li, Z.; Ji, M.; Zhao, M.; Shen, M.; Han, X.; Jia, T.; Li, C.; Wang, Y., *Adv. Funct. Mater.* **2021,** *31*, 2106247.

S3 Zhao, M.; Zhu, Y.; Pan, Y.; Wang, Y.; Xu, T.; Zhao, X.; Jia, T.; Zhang, Z.; Chen, Z., *ACS Appl. Energy Mater.* **2022,** *5*, 15758-15767.

S4 Prakoso, S. P.; Sun, S. S.; Saleh, R.; Tao, Y. T.; Wang, C. L., *ACS Appl. Mater. Interfaces* **2021,** *13*, 38365-38374.

S5 Li, H.; Wen, H.; Li, J.; Huang, J.; Wang, D.; Tang, B. Z., *ACS Appl. Mater. Interfaces* **2020,** *12*, 26033-26040.

S6 Chen, G.; Sun, J.; Peng, Q.; Sun, Q.; Wang, G.; Cai, Y.; Gu, X.; Shuai, Z.; Tang, B. Z., *Adv. Mater.* **2020,** *32*, e1908537.

S7 Zhang, X.; Li, Y.; Chen, Z.; Li, P.; Chen, R.; Peng, X., *Dyes Pigm.* **2021,** *192*, 109460.

S8 Dai, J.; Qi, S.; Zhao, M.; Liu, J.; Jia, T.; Liu, G.; Liu, F.; Sun, P.; Li, B.; Wang, C.; Zhou, J.; Lu, G., *Chem. Eng. J.* **2023,** *471*, 144745.

S9 Zhang, R.; Jin, N.; Jia, T.; Wang, L.; Liu, J.; Nan, M.; Qi, S.; Liu, S.; Pan, Y., *J. Mater. Chem. A* **2023,** *11*, 15380-15388.